Langmuir

Article

pubs.acs.org/Langmuir

In Situ Formation and Size Control of Gold Nanoparticles into Chitosan for Nanocomposite Surfaces with Tailored Wettability

Fabrizio Spano,*[,†] Alessandro Massaro,[†] Laura Blasi,[‡] Mario Malerba,[§] Roberto Cingolani,[§] and Athanassia Athanassiou*[,†,‡,§]

[†]Center for Biomolecular Nanotechnologies @UNILE, Istituto Italiano di Tecnologia (IIT), via Barsanti, 73010 Arnesano, Lecce, Italy

[‡]National Nanotechnology Laboratory (NNL), CNR-Istituto Nanoscienze, via per Arnesano 73100 Lecce, Italy

[§]Istituto Italiano di Tecnologia (IIT), via Morego 30, 16163 Genova, Italy

Supporting Information

ABSTRACT: The in situ formation of gold nanoparticles into the natural polymer chitosan is described upon pulsed laser irradiation. In particular, hydrogel-type films of chitosan get loaded with the gold precursor, chloroauric acid salt ($HAuCl_4$), by immersion in its aqueous solution. After the irradiation of this system with increasing number of ultraviolet laser pulses, we observe the formation of gold nanoparticles with increasing density and decreasing size. Analytical studies using absorption measurements, atomic force microscopy, scanning electron microscopy, and X-ray photoelectron spectroscopy of the nanocomposite samples throughout the irradiation procedure reveal that under the specific irradiation conditions there are two competing mechanisms responsible for the nanoparticles production: the photoreduction of the precursor responsible for the rising growth of gold particles with increasing size and the subsequent photofragmentation of these particles into smaller ones. The described method allows the localized formation of gold nanoparticles into specific areas of the polymeric films, expanding its potential applications due to its patterning capability. The size and density control of the gold nanoparticles, obtained by the accurate increase of the laser irradiation time, is accompanied by the simultaneously controlled increase of the wettability of the obtained gold nanocomposite surfaces. The capability of tailoring the hydrophilicity of nanocomposite materials based on natural polymer and biocompatible gold nanoparticles provides new potentialities in microfluidics or lab on chip devices for blood analysis or drugs transport, as well as in scaffold development for preferential cells growth.

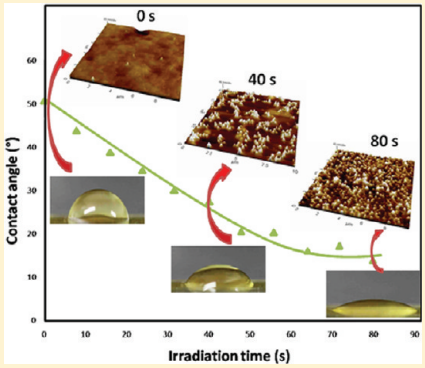

INTRODUCTION

Control of surface wettability is desirable in various applications expanding in a wide range of domains as industry, biology, and medicine,[1−6] especially if the surfaces can be modified by a simple technique. Controlling the wettability is also possibly the simplest approach for managing the liquid flow in microfluid devices,[7] since the flow is strongly affected by the surface wetting characteristics of the walls of the capillaries. Indeed, water can be easily introduced into hydrophilic microchannels, while, in the case of hydrophobic channels, additional external pressure is required. For this reason, different techniques for the control of the wettability have been developed in microfluidics for chemical and biochemical analysis.[8−14] By the use of nanocomposite materials, combining the properties of polymers and nanofillers, hydrophobic polymers can be turned into hydrophilic nanocomposite materials, preserving their flexibility and easy processability. In this work, we demonstrate the fine control of the surface properties of a nanocomposite system using laser irradiation. The studied system, is a film of the natural polymer chitosan (CTO) (its molecular structure is illustrated in Figure 1a) into which is introduced the chloroauric acid salt ($HAuCl_4$) by immersion.[15] CTO is a natural biodegradable and biocompatible polysaccharide polymer derived from chitin (the second most naturally abundant polysaccharide on the planet to cellulose), a linear chain of acetylglucosamine groups, extracted from crustacean shells and the cell walls of many fungi. For these reasons, it is ideal for biological applications. The process of the precursor salt loading into the films is possible due to the ability of CTO polymer to behave as a hydrogel when used in high concentrations.[16−18] Indeed, this hydrogel nature of CTO results in the tendency to absorb ambient moisture or liquid solutions. After the precursor loading and upon UV irradiation the creation of gold nanoparticles (Au NPs) occurs, exclusively in the irradiated areas of the polymeric film, making possible the patterning of this composite material. Moreover, the tuning of the size of the formed metallic particles in the nanoscale is achieved, by adjusting the laser parameters, such as irradiation time. A reported work has attributed the formation of gold particles of nanometer-size in CTO films upon UV lamp irradiation to the

Received: October 5, 2011
Revised: January 27, 2012
Published: January 31, 2012

   dx.doi.org/10.1021/la203893h | Langmuir 2012, 28, 3911−3917

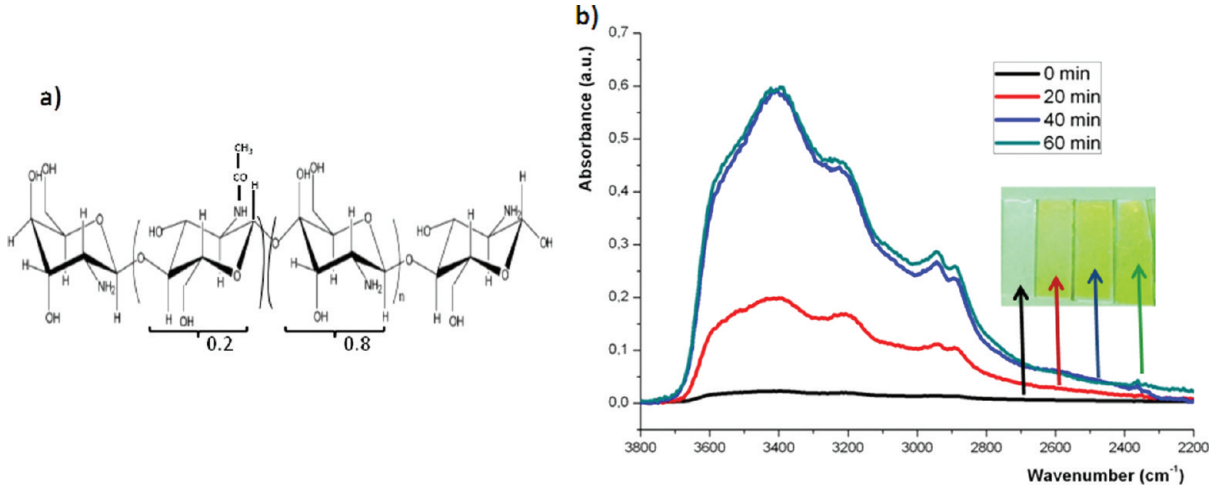

Figure 1. (a) Chemical structure of chitosan and (b) FT-IR absorption of CTO polymer films incorporating different amounts of Au precursor, due to different immersion times into the solution of the latter. The spectra indicate the hydrogel nature of the CTO polymer illustrated by its ability to absorb Au precursor. The inset shows pictures of CTO polymer films on glass substrates with increasing precursor concentration from left to right.

photoreduction of the salt precursor into gold atoms, which clusterize and eventually form gold particles. In that work the size of the formed particles increased upon increasing irradiation time.[15] In contrast, we demonstrate that increasing UV irradiation creates Au particles with decreasing size. We prove that this effect is due to two mechanisms that occur simultaneously in our samples due the UV pulsed laser irradiation: photoreduction and photofragmentation. Photofragmentation of metallic nanoclusters into particles with sizes ranging from 60 to 5 nm is previously reported in liquid using pulsed laser excitation.[19−22] This is the first reported system where the mechanism of photofragmentation competes with the photoreduction, resulting in an increasing density of Au NPs with decreasing sizes in CTO films upon UV irradiation. Finally, we have correlated the wettability changes in the nanocomposite system upon irradiation with the Au NPs density and size-control process, opening the way to numerous applications in fluidic systems, cells growth, drug delivery, etc.

EXPERIMENTAL SECTION

For the preparation of the polymeric films, 75−85% deacetyled CTO polymer (Sigma Aldrich, cat. no. 448877) was initially dissolved in acetic acid (1 wt % in distilled water; Sigma Aldrich, cat. no. 242853). CTO is soluble in weak acids due to the low pK_a of approximately 6.5, and once in solution, protonation of the amino groups gives CTO a cationic nature.[23] Various concentrations of CTO polymer solutions (0.5 and 1 wt %) were prepared. CTO polymeric films were obtained by drop-casting (50 μL/cm^2) on glass substrates. The use of the specific CTO concentrations allows the formation of CTO hydrogels able to absorb the Au precursor. The precursor used is a chloroauric acid salt (Sigma Aldrich, cat. no. 254169; M_w(HAuCl$_4$) = 339.5 g/mol) that was dissolved in distilled water ([Au] = 0.01M). The precursor was introduced in the CTO polymeric film by immersion of the latter in the water solution of the former. Different immersion times allowed tuning of the precursor concentration introduced into the CTO polymeric films. The thickness of the CTO films obtained by drop-casting is between 1.5 and 5.0 μm and is a function of the CTO solution concentration.[24] The generation of Au NPs does not occur during the immersion phase. For the initiation of the formation of the Au NPs precursor the use of UV light is essential. The light source used is a pulsed Nd:YAG laser (Quanta-Ray GCR-190, Spectra Physics) operating at 10 Hz with 4−6 ns pulse duration. The wavelength used for all our experiments is 355 nm. The laser irradiation is realized at room temperature with a relative humidity of 30−60%.

Absorption spectra of the CTO−Au NPs films were performed with a UV−visible spectrophotometer (VARIAN Cary 300 Scan). Fourier transform infrared spectroscopy (FT-IR) spectra were realized with a VERTEX 70 FT-IR instrument in the spectral range defined from 4000 to 1500 cm^{-1} in absorbance mode. For atomic force microscopy (AFM) images, a Park System AFM instrument (XE-100) was used in true noncontact mode. The images were realized in air using an antivibration table (Table Stable TS-150) and an acoustic enclosure. Single-beam silicon cantilevers tips (PPP-NCHR-10) were used for the data acquisition with about less than 10 nm nominal radius and 42 N/m elastic force constant for high sensitivity. The resonance frequency was defined around 280 kHz. The scan rate was between 0.2 and 1.0 Hz. Optical microscopy images were realized with a Zeiss AXIO instrument. Scanning electron microscopy (SEM) images were taken using a FEI NOVA nanoSEM 200 scanning electron microscope. The measurements were realized in low vacuum with a pressure of 30 Pa by using a Helix detector at a tension of 30 kV. Apparent contact angle measurements were done using a KSV CAM 200 instrument. The sessile drop method was employed using distilled water with a typical drop volume around 1 μL. All the apparent water contact angle measurements are done in equilibrium 30 s after the droplet deposition. X-ray photoelectron spectroscopy (XPS) measurements were made using a Specs Lab2 electron spectrometer with a monochromatic X-ray source radiation at 1253 eV and equipped with an Phoibos analyzer Has 3500 (Emispherical energy analyzer). The tension of the X-ray source Mg Kα was 10 kV for the wide scan (with an energy step of 0.5) and 12 kV for the spectroscopic scan (with an energy step of 0.2). The pass energy was 90 eV.

RESULTS AND DISCUSSION

The gold precursor was introduced in the CTO polymer thin films varying the immersion time of the films in the precursor solution. In this way different composite hydrogel samples were obtained with varying precursor concentrations. Indeed, in Figure 1b are illustrated FT-IR spectra of CTO films of thickness 1.5 μm (starting solution 0.5 wt % CTO in acetic acid) with increasing precursor concentrations, obtained after increasing immersion times (from 20 to 60 min) in the precursor solutions ([Au] = 0.01 M).[24] The increase in the absorption intensity of the curves obtained after 40 or 60 min of immersion with respect to the one obtained after 20 min of immersion clearly demonstrates the increased precursor concentration in the case of longer immersion times. The superposition of the FTIR curves of the samples obtained after 40 and 60 min of immersion indicates the saturation of the precursor concentration in these films. All the CTO-based samples that will be presented herein have been obtained after

dx.doi.org/10.1021/la203893h | Langmuir 2012, 28, 3911−3917

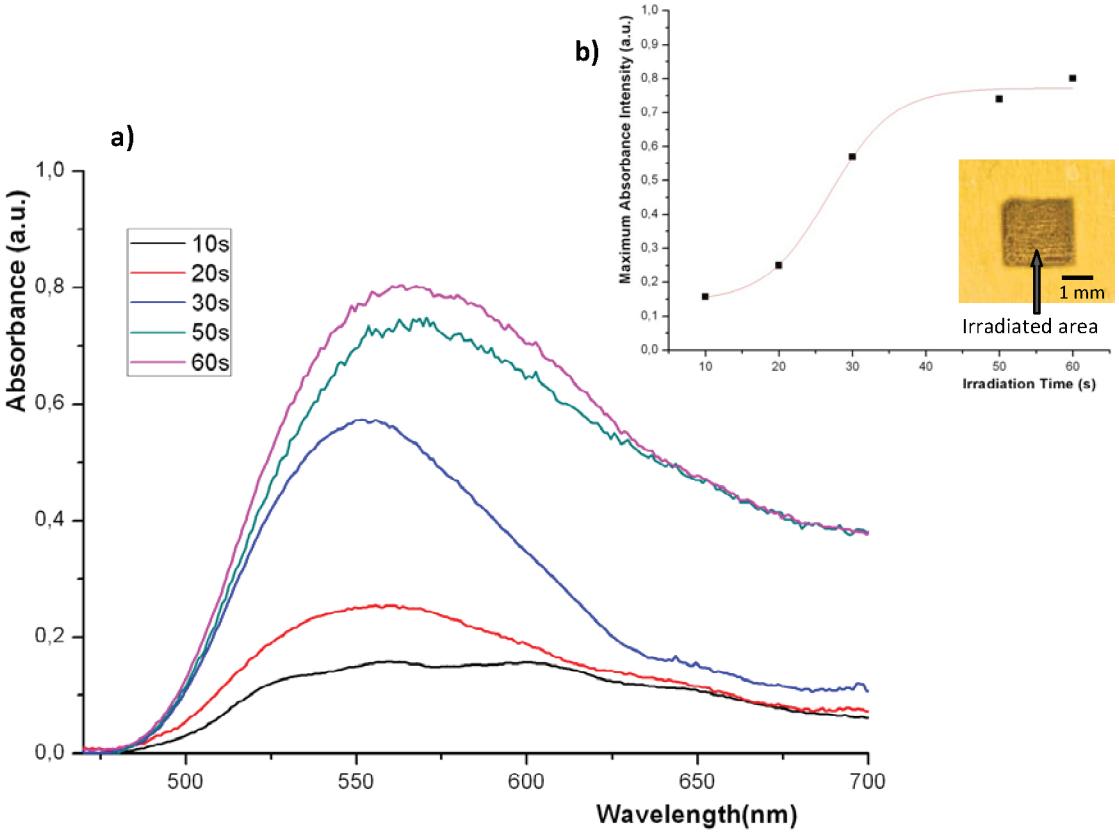

Figure 2. (a) UV−visible spectra of CTO films incorporating Au precursor after different UV irradiation times (10−60 s, fluence = 30 mJ·cm^{-2}). (b) Maximum absorbance intensity of the nanocomposite films as a function of their irradiation time. The fit is done using the sigmoidal function. The inset shows a photo of a CTO−Au precursor film after its irradiation through a mask of 2.2 × 2.3 mm^2 for 80 s.

immersion times long enough to ensure saturation loading of the precursor. Films obtained from CTO acetic acid solutions with concentrations of 1.0 wt % or higher have increased thickness in comparison with the films obtained from 0.5 wt % CTO in acetic acid. As the thickness increases, the amount of the gold precursor absorbed by the samples also increases, as shown in the Supporting Information (Figure 1s). All the films that will be presented herein were obtained from a solution of 0.5 wt % CTO in acetic acid useless otherwise stated.

CTO polymer is known to be a reducing agent of Au precursors.[25] Nevertheless, in our case, as the precursor is introduced after the formation of the CTO films and not in solution, the reduction process needs to be stimulated by an external excitation. The use of UV laser light allows us to generate photolytic Au NPs in the CTO polymer film. Moreover, the generation occurs exclusively at precise areas where laser interacts with the samples. The color in the irradiated films varies from pale blue-violet to a clear gold with increasing irradiation times, and especially for short irradiation times, it appears with a delay after the termination of the irradiation. Therefore, the irradiated systems demonstrate a "relaxation time" needed to obtain the complete photolytic reaction, and its full study will be addressed elsewhere. In the presented experiments all the characterizations were performed 24 h after the completion of the irradiation procedure. Figure 2a shows UV−vis spectra obtained from a CTO−Au precursor film after different irradiation times, with the absorption band of the formed gold appearing around 520−620 nm.[26,27] The monitored spectra are quite broad, indicating the broad size distribution of the generated particles throughout the samples. The evolution of the maximum absorbance intensity versus the irradiation time follows a trend, indicating a saturation behavior illustrated by a plateau obtained after 50−60 s irradiation time, as demonstrated in Figure 2b. The inset of this figure shows an image of a CTO sample incorporating Au precursor after its irradiation at the central area for 80 s. The creation of Au NPs occurs exclusively in the irradiated area of the polymeric film, demonstrating the patterning capability of the proposed system. The exclusive Au NPs formation in the UV-irradiated areas can also be seen in the AFM images presented in the Supporting Information (Figure 2s), which show the interface between an irradiated (left) and a nonirradiated (right) area.

The generation of Au NPs at the surface of the nanocomposite films as a function of the irradiation time was examined by atomic force microscopy. Figure 3a−c illustrates a nonirradiated area of a CTO film incorporating the salt precursor of gold, indicating a very smooth surface with a roughness of a few nanometers. In the absence of laser irradiation, no particles are observed on the surface of the CTO polymeric films. Figure 3d−f represents an area of the same film after 20 s of laser irradiation with a laser fluence of 30 mJ·cm^{-2}. At this stage, the generation of Au NPs is clear with an average size around 500 nm, as illustrated in the higher magnification AFM images shown in Figure 4a−c. By increasing the irradiation time to 80 s (Figure 3g−i), the Au NPs density seems to increase with a parallel reduction of their size. From the higher magnification images shown in Figure 4d−f, the average diameter of the nanoparticles is estimated around 100 nm. At the specific fluence, after 80 s of irradiation, the Au NPs formed on the surface of the samples become very dense and form a sort of continuous surface film, as shown in Figure 3g−i. A careful

dx.doi.org/10.1021/la203893h | Langmuir 2012, 28, 3911−3917

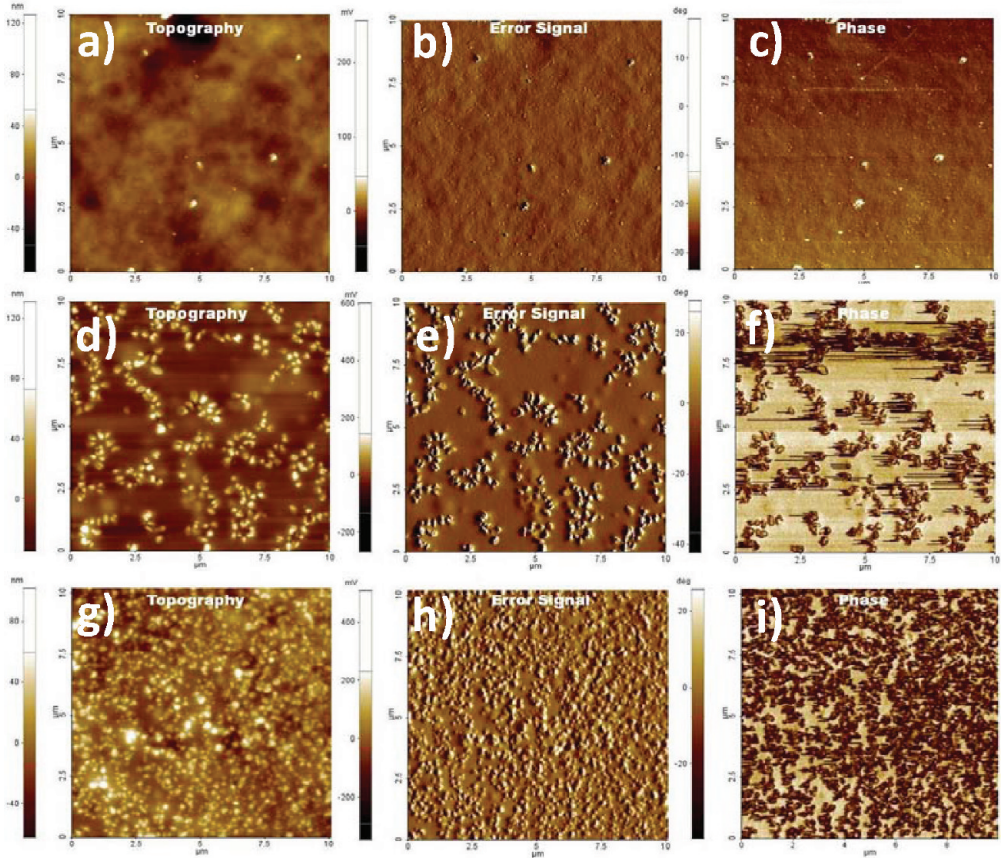

Figure 3. Evolution of the gold particles density and size for different irradiation times viewed by AFM images. Topography, error, and phase AFM images for an area (a–c) without irradiation, (d–f) after 20 s laser irradiation, and (g–i) after 80 s laser irradiation.

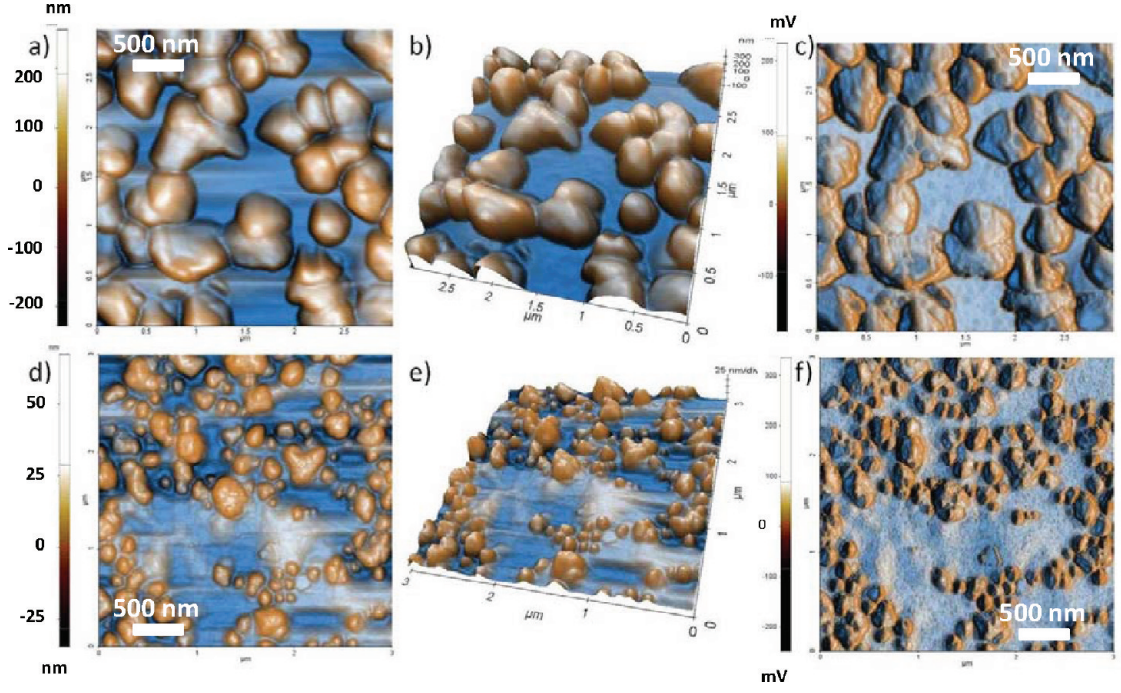

Figure 4. High-resolution atomic force microscopy images illustrating the size variation of Au NPs in CTO composite films: (a) topography, (b) 3D topography, and (c) error signal images after 20 s laser irradiation and (d) topography, (e) 3D topography, and (f) error signal images after 80 s laser irradiation.

examination of the shape of the formed NPs reveals that they adopt spherical shapes after prolonged irradiation (Figure 4d–f), whereas upon smaller irradiation times they seem more irregular (Figure 4a–c). The analysis of the AFM phase images (Figure 3c,f,i) indicates a phase variation at the precise positions of the Au NPs, demonstrating that they are exposed to air and are not

dx.doi.org/10.1021/la203893h | *Langmuir* 2012, 28, 3911–3917

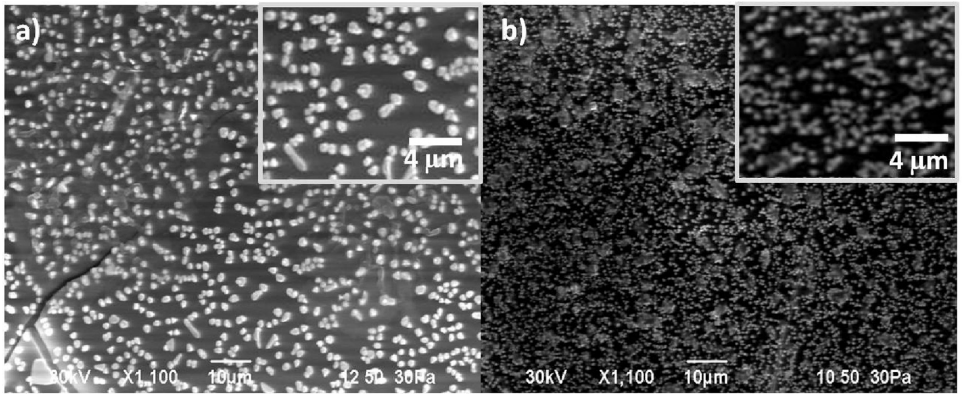

Figure 5. (a) SEM image of a CTO composite surface after 20 s irradiation time showing the presence of Au NPs. The inset shows a magnified image, from which the average size of Au NPs can be estimated to be around 500 nm. (b) SEM image of a CTO composite surface after 80 s irradiation time showing the presence of Au NPs. The inset shows a magnified image from which the average size of Au NPs can be estimated to be around 100 nm.

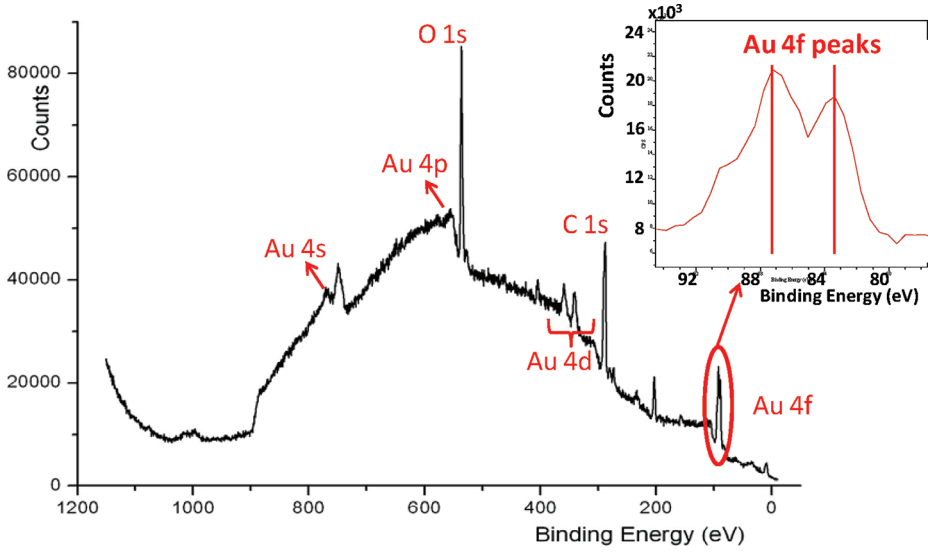

Figure 6. XPS spectrum of the CTO−Au precursor film after 80 s of laser irradiation illustrating the presence of the Au 4f peak, characteristic of the formed Au NPs. The inset shows a magnified spectrum of the dual Au 4f peak.

covered by a polymeric layer. Further increase of the irradiation time above 80 s seems to induce a melting and eventually a burning effect to the nanocomposite materials. AFM images shown in the Supporting Information [Figure 3s(a−c)] demonstrate a nanocomposite film after 3 min irradiation. It can be clearly seen that a blend of Au particles and CTO polymer is formed, where the Au NPs become difficult to discriminate, most likely due to the melting mechanism.

For a further confirmation of the AFM observations and a verification of the nature of the formed NPs, we performed scanning electron microscopy analysis and XPS measurements on samples formed and irradiated with the same conditions as those used for the AFM measurements. SEM images of the CTO−Au NPs films after two different irradiation times are shown in Figure 5. In particular, parts a and b of Figure 5 respectively illustrate the SEM images after 20 and 80 s laser irradiation. The comparison of these two areas confirms the AFM observations for the variation in size and density of the Au NPs generated by laser irradiation, with decreasing particle size and increasing density upon increasing irradiation time. The XPS spectrum of an area of the film irradiated for 80 s (Figure 6) allows us to verify the presence of Au NPs by means of the Au 4f peak observed around 86 eV.[28,29] The inset of Figure 6 illustrates the characteristic dual peak of Au 4f.

The growth of Au NPs in CTO films has been previously observed and attributed to agglomeration and cluster formation of the gold atoms produced due to the photoreduction of their precursor.[15] Nevertheless, an exclusive agglomeration mechanism cannot be confirmed in our experiment since, in contrast with previous observations, the formed NPs decrease in size with increasing irradiation time, eventually forming NPs in the 100 nm range. This decrease of size may be correlated to a specific fragmentation mechanism occurring upon pulsed laser irradiations. Several works[30−38] indicate the formation of metal nanoparticles by pulsed laser ablation of solid metal targets in liquid solutions. The average diameter of the particles decreases with the irradiation time. The major mechanism used to describe this decreasing size behavior is the fragmentation of previously formed particles by self-absorption of laser pulses. A theoretical work indicates also the possibility to melt small gold particles under thermal annealing.[38] Correlated with the size reduction and the shape changes of the produced NPs observed in our experiments upon pulsed laser irradiation, all the above-mentioned mechanisms can simultaneously occur in our system.

dx.doi.org/10.1021/la203893h | *Langmuir* 2012, 28, 3911−3917

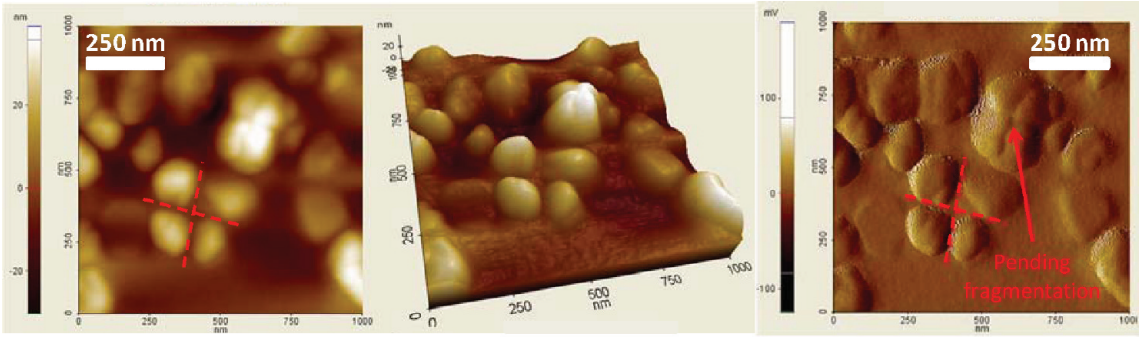

Figure 7. (a) Topography, (b) 3D topography, and (c) error signal AFM images of CTO−Au precursor samples after 70 s irradiation time (laser irradiation fluence = 30 mJ·cm^{-2}). The images illustrate particles that seem to result after the fragmentation of bigger ones (see red cross), while others seem to be in the process of fragmentation (see red arrow).

To demonstrate this hypothesis, we present a comprehensive analysis of AFM images performed on a nanocomposite sample irradiated with 30 mJ·cm^{-2} for 70 s, close to the condition for the full coverage of the nanocomposite surface with Au NPs (inset in Figure 2 and Figure 3g−i). Indeed, in Figure 7 detailed AFM images of the formed Au NPs clearly indicate that the majority of the particles are the result of fragmentation of bigger ones. Some of them are in the process of fragmentation and others are already fragmented and start to separate, indicating a mobility mechanism most likely related to the hydrogel nature of the CTO matrix and to the size of the formed NPs. During the fragmentation mechanism, upon absorption of laser pulses an increase of local temperature may occur that can increase further the mobility of the Au NPs in the CTO polymeric film.[15] This mobility may allow some of the NPs to reach the surface of the CTO polymer film even if they are created in the bulk.

The change in the size and the density of the formed Au NPs upon laser irradiation strongly affects the wettability properties of the nanocomposite surfaces. By tuning the irradiation parameters the wetting properties of the formed surfaces can be precisely controlled in order to be implemented in diverse applications, as controlled flow of liquids, direction growth of biological molecules, etc. Indeed, Figure 8 demonstrates the

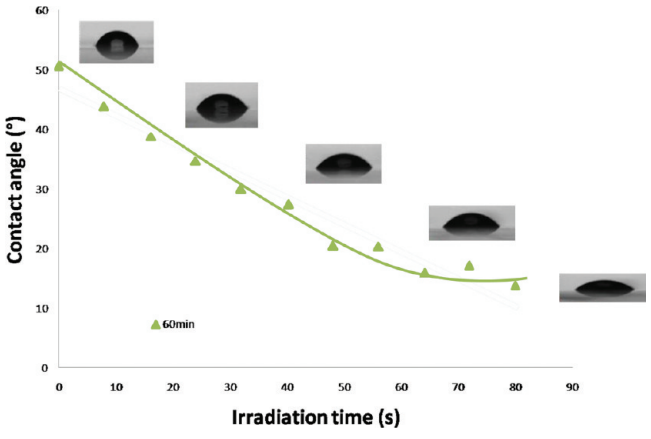

Figure 8. Apparent water contact angle measurements on CTO−Au precursor films as a function of their irradiation time (fluence = 30 mJ·cm^{-2}). The corresponding water droplets images are also shown.

apparent water contact angle (AWCA) values of the previously analyzed nanocomposite systems, as a function of the irradiation time. The AWCA decreases as a function of the increasing irradiation time by ≈40°, starting from more than 50° ± 2° for the nonirradiated samples and arriving to the superhydrophilic value of 13° ± 2° after 80 s irradiation. The insets of the same figure show the photos of the droplets lying on each measured area. AWCA measurements on another composite sample starting from 1.0 wt % CTO in acetic acid show that prolonged irradiation times above 80 s result in an important increase of the AWCA, reaching almost 90° ± 2° after 180 s (Figure 4s). This can be explained by the melting, burning, and eventually even ablation of the nanocomposite, creating a fused sample of polymer and Au particles (previously reported in the Supporting Information, Figure 3s) with diverse roughness and altered chemistry. The results clearly demonstrate the potentiality of the technique to tune the surface wettability of the Au NPs/CTO nanocomposites by controlling the irradiation time.

CONCLUSIONS

In this work we describe the formation of patterns of gold nanoparticles in solid chitosan films by laser irradiation. We illustrate the simultaneous density growth and size reduction of the gold nanoparticles as a function of the laser irradiation time. We introduce the hypothesis of two synchronized mechanisms, i.e., nucleation of the photoreduced gold atoms and photofragmentation of the formed clusters, with the former being responsible for the density growth and the latter for the size reduction of the gold particles. The fine control over the morphology of the surface of the Au NPs/CTO nanocomposites allows also the tuning of the surface wettability of the films, by changing the laser irradiation time. Indeed, by controlling the hydrophilicity we open the way for the use of this biocompatible system in microfluidic applications, scaffolds for cells growth, etc.

ASSOCIATED CONTENT

Supporting Information

Additional figures as noted in the text. This material is available free of charge via the Internet at http://pubs.acs.org.

AUTHOR INFORMATION

Corresponding Author

*E-mail: fabrizio.spano@iit.it (F.S.), athanassia.athanassiou@iit.it (A.A).

Notes

The authors declare no competing financial interest.

REFERENCES

(1) Comelles, J.; Estévez, M.; Martínez, E.; Samitier, J. *Nanomed.: Nanotechnol., Biol. Med.* **2010**, *6*, 44.
(2) Song, W.; Gaware, V. S.; Rúnarsson, Ö. V.; Másson, M.; Mano, J. F. *Carbohydr. Polym.* **2010**, *81*, 140.
(3) Rizzello, L.; Sorce, B.; Sabella, S.; Vecchio, G.; Galeone, A.; Brunetti, V.; Cingolani, R.; Pompa, P. P. *ACS Nano* **2011**, *5*, 1865.
(4) Winton, B. R.; Ionescu, M.; Lukey, C.; Wilson, M. R.; Nevirkovets, I. P.; Dou, S. X. *Adv. Sci. Lett.* **2011**, *4*, 431.
(5) Guo, Z.; Liu, W. *Appl. Phys. Lett.* **2007**, *90*, 223111.
(6) Rizzello, L.; Shankar, S. S.; Fragouli, D.; Athanassiou, A.; Cingolani, R.; Pompa, P. P. *Langmuir* **2009**, *25*, 6019.
(7) Villafiorita-Monteleone, F.; Canale, C.; Caputo, G.; Cozzoli, P. D.; Cingolani, R.; Fragouli, D.; Athanassiou, A. *Langmuir* **2011**, *27*, 8522.
(8) He, B.; Patankar, N. A.; Lee, J. *Langmuir* **2003**, *19*, 4999.
(9) Tsougeni, K.; Papageorgiou, D.; Tserepi, A.; Gogolides, E. *Lab Chip* **2010**, *10*, 462.
(10) Abate, A. R.; Krummel, A. T.; Lee, D.; Marquez, M.; Holtze, C.; Weitz, D. A. *Lab Chip* **2008**, *8*, 2157.
(11) Sun, C.; Zhao, X.; Han, Y.; Gu, Z. *Thin Solid Films* **2008**, *516*, 4059.
(12) Bayiati, P.; Tserepi, A.; Petrou, P. S.; Kakabakos, S. E.; Misiakos, K.; Gogolides, E. *J. Appl. Phys.* **2007**, *101*, 103306.
(13) Luk, V. N.; Mo, G. CH.; Wheeler, A. R. *Langmuir* **2008**, *24*, 6382.
(14) Nagai, H.; Irie, T.; Takahashi, J.; Wakida, S. *Biosens. Bioelectron.* **2007**, *22*, 1968.
(15) Miyama, T.; Yonezawa, Y. *Langmuir* **2004**, *20*, 5918.
(16) Goycoolea, F. M.; Argüelles-Monal, W. M.; Lizardi, J.; Peniche, C.; Heras, A.; Galed, G.; Díaz, E. I. *Polym. Bull.* **2007**, *58*, 225.
(17) Ta, H. T.; Dass, C. R.; Dunstan, D. E. *J. Controlled Release* **2008**, *20*, 205.
(18) Ishihara, M.; Obara, K.; Nakamura, S.; Fujita, M.; Masuoka, K.; Kanatani, Y.; Takase, B.; Hattori, H.; Morimoto, Y.; Ishihara, M.; Maehara, T.; Kikuchi, M. *J Artif. Organs* **2006**, *9*, 8.
(19) Kamat, P. V. *Phys. Chem. B* **2002**, *106*, 7729.
(20) Kamat, P. V.; Flumiani, M.; Hartland, G. *J. Phys. Chem. B* **1998**, *102*, 3123.
(21) Dawson, A.; Kamat, P. V. *J. Phys. Chem. B* **2001**, *105*, 960.
(22) Fujiwara, H.; Yanagida, S.; Kamat, P. V. *J. Phys. Chem. B* **1999**, *103*, 2589.
(23) Ercolessi, F.; Andreoni, W.; Tosatti, E. *Phys. Rev. Lett.* **1991**, *66*, 911.
(24) Spano, F.; Massaro, A.; Cingolani, R.; Athanassiou, A. *Microelectron. Eng.* **2011**, *88*, 2763.
(25) Huang, H.; Yuan, Q.; Yang, X. *J. Colloid Interface Sci.* **2005**, *282*, 26.
(26) Duff, D. G.; Baiker, A.; Edwards, P. P. *Langmuir* **1993**, *9*, 2301.
(27) Bertino, M. F.; Sun, Z.-M.; Zhang, R.; Wang, L.-S. *J. Phys. Chem. B* **2006**, *110*, 21416.
(28) Tuzovskaya, I.; Bogdanchikova, N.; Simakov, A.; Gurin, V.; Pestryakov, A.; Avalos, M.; Farias, M. H. *Chem. Phys.* **2007**, *338*, 23.
(29) Baoqiang, L.; Xiaodong, S.; Yang, L.; Yi, L.; Jianfei, M.; Xiao, D. *Inorg. Mater.* **2008**, *44*, 813.
(30) Kalyva, M.; Bertoni, G.; Milionis, A.; Cingolani, R.; Athanassiou, A. *Microsc. Res. Tech.* **2010**, *73*, 937.
(31) Mafuné, F.; Kohno, J.; Takeda, Y.; Kondow, T.; Sawabe, H. *J. Phys. Chem. B* **2001**, *105*, 5114.
(32) Mafuné, F.; Kohno, J.; Takeda, Y.; Kondow, T. *J. Phys. Chem. B* **2000**, *104*, 8333.
(33) Mafuné, F.; Kohno, J.; Takeda, Y.; Kondow, T.; Sawabe, H. *J. Phys. Chem. B* **2000**, *104*, 9111.
(34) Shukla, S.; Seal, S. *Nanostruct. Mater.* **1999**, *11* (8), 1181.
(35) Videla, F. A.; Torchia, G. A.; Schinca, D. C.; Scaffardi, L. B.; Moreno, P.; Méndez, C.; Giovanetti, L. J.; Ramallo Lopez, J. M.; Roso, L. *J. Appl. Phys.* **2010**, *107*, 114308.
(36) Kadossov, E.; Burghaus, U. *Catal. Lett.* **2010**, *134*, 228.
(37) Kabashin, A. V.; Meunier, M. *J. Appl. Phys.* **2003**, *94*, 7941.
(38) Barcikowski, S.; Hahn, A.; Kabashin, A. V.; Chichkov, B. N. *Appl. Phys. A: Mater. Sci. Process.* **2007**, *87*, 47.